# Photomodulation of Two-Dimensional Self-Assembly of Azobenzene−Hexa-*peri*-hexabenzocoronene−Azobenzene Triads

Ian Cheng-Yi Hou,[†] Valentin Diez-Cabanes,[‡] Agostino Galanti,[§] Michal Valášek,[∥] Marcel Mayor,[∥,⊥] Jérôme Cornil,[‡] Akimitsu Narita,*[†,#] Paolo Samorì,*[§] and Klaus Müllen*[†,∇]

[†]Max Planck Institute for Polymer Research, Ackermannweg 10, D-55128 Mainz, Germany

[‡]Laboratory for Chemistry of Novel Materials, University of Mons, Place du Parc 20, B-7000 Mons, Belgium

[§]Université de Strasbourg, CNRS, ISIS UMR 7006, 8 allée Gaspard Monge, 67000 Strasbourg, France

[∥]Institute of Nanotechnology, Karlsruhe Institute of Technology KIT, P.O. Box 3640, 76021 Karlsruhe, Germany
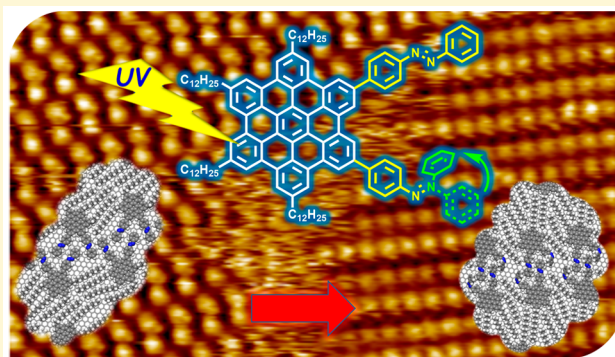
[⊥]Department of Chemistry, University of Basel, St. Johannsring 19, 4056 Basel, Switzerland

[#]Organic and Carbon Nanomaterials Unit, Okinawa Institute of Science and Technology Graduate University 1919-1 Tancha, Onna-son, Kunigami, Okinawa 904-0495, Japan

[∇]Institute of Physical Chemistry, Johannes Gutenberg-University Mainz, Duesbergweg 10-14, D-55128 Mainz, Germany

**S** Supporting Information

**ABSTRACT:** Achieving exquisite control over self-assembly of functional polycyclic aromatic hydrocarbons (PAH) and nanographene (NG) is essential for their exploitation as active elements in (nano)technological applications. In the framework of our effort to leverage their functional complexity, we designed and synthesized two hexa-*peri*-hexabenzocoronene (HBC) triads, *p*AHA and *o*AHA, decorated with two light-responsive azobenzene moieties at the pseudo-*para* and *ortho* positions, respectively. Their photoisomerization in solution is demonstrated by UV−vis absorption. ¹H NMR measurements of *o*AHA suggested 23% of *Z*-form can be obtained at a photostationary state with UV irradiation (366 nm). Scanning tunneling microscopy imaging revealed that the self-assembly of



*p*AHA and *o*AHA at the solid−liquid interface between highly oriented pyrolytic graphite (HOPG) and their solution in 1,2,4-trichlorobenzene can be modulated upon light irradiation. This is in contrast to our previous work using HBC bearing a single azobenzene moiety, which did not show such photomodulation of the self-assembled structure. Upon *E*-*Z* isomerization both *p*AHA and *o*AHA displayed an increased packing density on the surface of graphite. Moreover, *p*AHA revealed a change of self-assembled pattern from an oblique unit cell to a dimer row rectangular crystal lattice whereas the assembly of *o*AHA retained a dimer row structure before and after light irradiation, yet with a modification of the inter-row molecular orientation. Molecular mechanics/molecular dynamics simulations validated the self-assembly patterns of *p*AHA and *o*AHA, comprising azobenzenes in their *Z*-forms. These results pave the way toward use of suitably functionalized large PAHs, as well as NGs, to develop photoswitchable devices.

## ■ INTRODUCTION

Hexa-*peri*-hexabenzocoronene (HBC), a molecule containing 42 sp² carbons and possessing a $D_{6h}$ symmetry, is one of the most representative and well-studied polycyclic aromatic hydrocarbons (PAHs). With a diameter slightly exceeding 1 nm, it is considered one of the smallest possible nanographenes (NGs), i.e., molecularly defined subunits of the graphene lattice which is confined in at least one of its lateral dimensions.[1−3] For this reason, HBC is frequently used as a model system to gain insight into the behavior of NG-based materials.[4−8]

The large π-conjugated core of HBC gives rise to strong, noncovalent interactions among adjacent molecules, as well as

between molecules and the basal plane of graphite. Understanding the resulting self-assembly processes is essential for advances in HBC-based (nano)technologies.[5,6,9] Self-assembly of HBC derivatives has been studied in various environments, namely, in solution and in bulk, where 3D columnar supramolecular structures are formed,[6,10−17] and on surfaces, enabling programmed 2D nanopatterning.[14,18,19] Substituents at peripheral positions play a key role in controlling self-

assembly behavior of HBC. For example, HBCs with appropriate alkyl substituents show thermal phase transitions between crystalline and liquid-crystalline phases, where the phase-transition temperature can be tuned by the length of the side chains.[6,11,20,21] Self-assembly of HBCs can thus be controlled by heat, yet the use of other external stimuli as remote controls to regulate self-assembly of HBC-based materials has only been occasionally considered.[19,22]

Among external stimuli, light is particularly attractive, as photons may be remotely applied with high spatial and temporal resolution. A plausible way of imparting photo-switchable characteristics to HBCs is to functionalize their peripheries with photochromic moieties.[23−26] In particular, azobenzene exhibits a pronounced geometric change between its *E/Z*-isomers, which has been applied to light-controllable, self-assembled materials and photomechanical devices.[27−31] Photoresponsive self-assembly of azobenzene-containing materials has been intensively investigated, especially at solid−air[32−36] and solid−liquid[19,37−42] interfaces. Surface confinement restricts assembly in 2D and provides an opportunity for detailed examination of structures and dynamics of these molecules in real space by scanning probe microscopy techniques. In this context, it is extremely interesting to combine carbon-based nanostructures with photochromic molecules like azobenzene to develop optically responsive systems and materials.[26] HBC bearing one azobenzene unit was previously reported, but self-assembly of its *Z*-form could not be observed on a graphite surface by scanning tunneling microscopy (STM).[19] Here we synthesized azobenzene−HBC−azobenzene triads, *p*AHA and *o*AHA (Scheme 1),

**Scheme 1. Synthesis of Azobenzene−HBC−Azobenzene *p*AHA and *o*AHA**



**1**, R$_1$ = *n*-dodecyl, R$_2$ = Br
**2**, R$_2$ = *n*-dodecyl, R$_1$ = Br
**3**

*p*AHA, 69%, R$_1$ = *n*-dodecyl, R$_2$ =
*o*AHA, 73%, R$_2$ = *n*-dodecyl, R$_1$ =

featuring an HBC core and two peripheral azobenzene moieties in the pseudo-*para* and pseudo-*ortho* positions, respectively. Geometries of *p*AHA and *o*AHA are employed to explore intermolecular interactions that affect their self-assembly. Photoisomerization of the azobenzene moieties in solution is confirmed by UV−vis absorption, combined with $^1$H NMR spectroscopy. Self-assembly of these two HBCs at the solid−liquid interface before and after UV light irradiation was monitored by STM and corroborated with molecular mechanics/molecular dynamics (MM/MD) simulations. Formation of stable self-assemblies for both *p*AHA and *o*AHA after isomerization of their azobenzene moieties reveals the potential of using large PAHs, as well as NGs, for photoresponsive devices and smart surfaces.

## ■ RESULTS AND DISCUSSION

**Synthesis of Azobenzene−HBC−Azobenzene Triads.** *p*AHA and *o*AHA were synthesized from the corresponding HBCs **1** and **2** bearing two bromo groups at desired positions,

in addition to four *n*-dodecyl chains,[43] which guarantee the molecule's good solubility in organic solvents and high affinity to graphite surfaces (Scheme 1). The azobenzene moieties were introduced by a 2-fold Suzuki coupling reaction between **1** or **2** with azobenzene boronic ester **3**.[44] *p*AHA and *o*AHA were isolated in 69% and 73% yields, respectively.

**Photoisomerization in Solution.** Reversible photo-isomerization of both *p*AHA and *o*AHA could be observed in solution upon alternating irradiation at 366 and 436 nm (Figures S1−S3). The spectral changes upon photoisomerization were relatively small and could be attributed to overlapping absorption features of the azobenzene units and the HBC core. HBC has a higher extinction coefficient,[15,45] which could overshadow spectral variation of the azobenzene units. Nevertheless, *o*AHA showed sufficient solubility to enable $^1$H NMR spectroscopic analysis at room temperature, which demonstrated that approximately 23% of *Z*-form was obtained in a photostationary state (PSS) after irradiation at 366 nm (Figure S4).

**STM Investigation of 2D Self-Assembly.** The UV−vis absorption and $^1$H NMR results, indicating the efficient photoisomerization of *p*AHA and *o*AHA in solution, motivated us to investigate the influence of isomerization on their self-assembly at the solid−liquid interface between graphite and their supernatant solutions. 2D self-assembly patterns of *p*AHA and *o*AHA were monitored by STM at the interface between 1,2,4-trichlorobenzene (TCB) solutions and highly oriented pyrolytic graphite (HOPG) before and after in situ UV light irradiation (Figures 1 and 2; Table 1). In all cases, brighter areas with a diameter of ∼1 nm can be assigned to HBC cores as a result of more favorable resonant tunneling between the Fermi level of HOPG and the frontier orbitals of the large aromatic core. Nonirradiated *p*AHA exhibits an oblique unit cell containing one molecule and an area of 6.8 ± 0.6 nm$^2$ per molecule (Figure 1a and Table 1), while *o*AHA forms a dimer-row structure with two molecules per unit cell and an area of 5.9 ± 0.3 nm$^2$ per molecule (Figure 2a and Table 1). A different assembly was also observed for *o*AHA (Figure S5; Table S1). These crystal packings are all assigned to assemblies of *E,E*-isomers, which have both azobenzenes in *E*-form (Figures 1a, 2a, and S5).

It is interesting to note that, although *p*AHA and *o*AHA are a pair of isomers themselves, their assemblies show significantly different density where that of *o*AHA is much more compact. Different packing motifs between *p*AHA and *o*AHA demonstrate that connectivity of the azobenzene−HBC−azobenzene triads strongly affects molecular self-assembly at the solid−liquid interface. The same supramolecular packing is extended over a larger area (50 nm × 50 nm) (Figures 1a and 2a, insets). Analysis of *p*AHA over even larger areas demonstrated that the crystalline domains end when terraces in the HOPG surface were encountered. These domains remained intact for hours without transforming into other self-assembled structures, thus confirming high stability of the crystal packing.

**STM Investigation after Light Irradiation.** After the 2D-self-assembly patterns of *p*AHA and *o*AHA were illustrated, their solution on the HOPG substrate was irradiated in situ with UV light ($\lambda_{irr}$ = 366 nm) to examine the effect of photoisomerization of the azobenzene moieties on the 2D crystalline assemblies. After 3 min of irradiation at a power density of 2 mW/cm$^2$, new domains with radically different lattice parameters were observed for both *p*AHA and *o*AHA, along with the simultaneous presence of the aforementioned
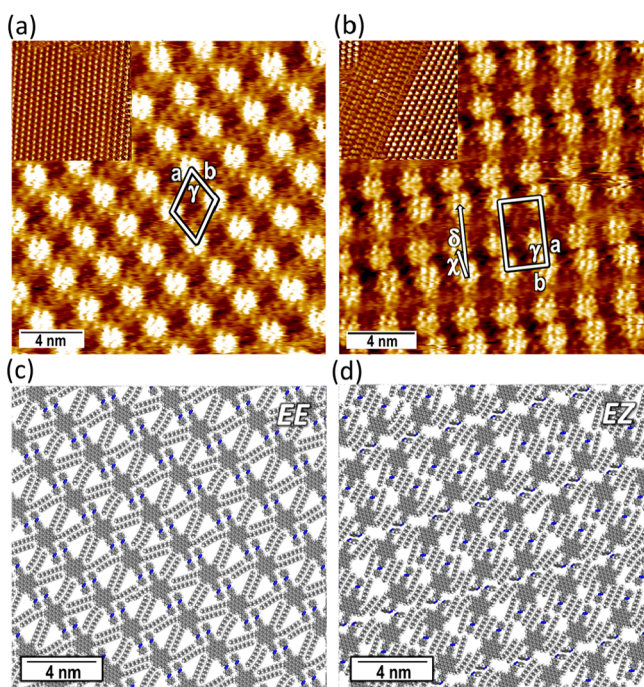
**Figure 1.** STM images recorded at the interface between HOPG and a 0.1 mM solution of *pAHA* in TCB and their 2D crystal packing models derived from MM/MD simulations. (a) An STM image taken without irradiation (*pAHA ori* in Table 1) and (c) a corresponding packing model of *E,E*-isomers. (b) An image recorded after irradiation at 366 nm (*pAHA irr* in Table 1) and (d) a corresponding packing model of *E,Z*-isomers. Inset in (a, b): images of the same crystal packing taken for a larger area of 50 nm × 50 nm. The newly formed dimer row crystal packing coexists with the oblique packing of *E,E*-isomers with a clear border, as can be seen in the inset of (b). Tunneling parameters: (a) bias voltage tunneling ($V_T$) = −300 mV, average tunneling current ($I_T$) = 20 pA; (c) $V_T$ = −300 mV, $I_T$ = 20 pA. Atom color coding: (c, d) carbon (gray), nitrogen (blue), hydrogen (white).

**Figure 2.** STM images recorded at the interface of HOPG and a 0.1 mM TCB solution of *oAHA* and their 2D crystal packing models derived from MM/MD simulations. (a) An STM image taken without irradiation (*oAHA ori* in Table 1) and (c) a corresponding packing model of *E,E*-isomers. (b) An image taken after irradiation at 366 nm (*oAHA irr* in Table 1) and (d) a corresponding packing model of *E,Z*-isomers. Inset in (a, b): images of the same crystal packing taken over a larger area 50 nm × 50 nm. The newly formed rectangular dimer row crystal packing coexists with the domain of *E,E*-isomers with a clear border, as can be seen in the inset of (b). Tunneling parameters: (a) $V_T$ = −550 mV, $I_T$ = 20 pA; (c) $V_T$ = −700 mV, $I_T$ = 20 pA. Atom color coding: (c,d) carbon (gray), nitrogen (blue), hydrogen (white).

domains formed by their *E,E*-isomers (Figures 1b and 2b, respectively). Molecules in the photomodified domains assemble in dimer rows with a rectangular crystal lattice for both *pAHA* and *oAHA* showing an area of 5.3 ± 0.2 nm² and 4.6 ± 0.3 nm² per molecule, respectively (Figures 1b and 2b and Table 1). Additionally, another dimer row structured self-assembly pattern with δ close to 0° and a parallelogram unit cell was observed for *pAHA* (Figure S6 and Table S1). HBC cores in the photomodified domains appear darker, compared with those in intact domains of the *E,E*-isomers, coexisting on the same STM image (inset of Figures 1b and 2b). This could indicate a larger HOPG/HBC distance[46] possibly induced by nonplanar *Z*-form azobenzene arms. Moreover, the photomodified domains exhibit denser packing than those in the original domains of the *E,E*-isomers, as evidenced by their smaller average area per molecule (Table 1). These observations support an assumption that the photomodified domains consist of molecules containing nonplanar *Z*-form isomers, with azobenzene arms presumably back-folded in the supernatant solution, reducing the molecular footprint visualized by STM. However, although rarely observed on HOPG for HBC species,[10,47,48] occurrence of a change in a 2D-assembly pattern for the *E,E*-isomers themselves cannot be completely excluded.
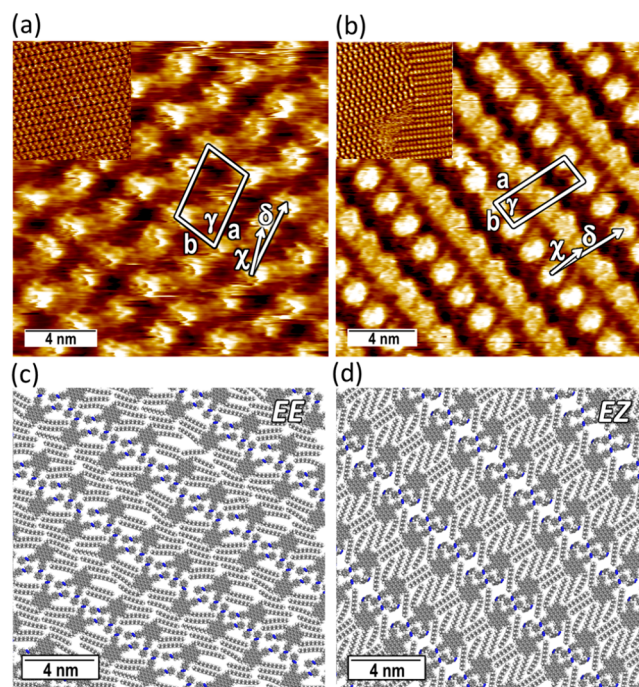
**Simulation of the Assembly Patterns.** MM/MD calculations were performed to further support the assumed formation of self-assembled domains consisting of isomers with *Z*-form azobenzenes, as well as to gain a greater understanding of how the azobenzene moieties govern the self-assembly of *pAHA* and *oAHA* by unraveling the packing at the atomistic level. Although lattice constants extracted from simulated results are generally larger than those experimentally determined, there is a reasonable agreement between experiment and simulation, allowing for a detailed interpretation of the STM images (Figure S7 and Table S2). Considering the relatively low *Z/E*-ratio at the PSS suggested by ¹H NMR measurements for *oAHA* (Figure S4) and assuming similar behavior for *pAHA*, we infer that the assembly patterns arising after irradiation in both cases are composed of *E,Z*-isomers, but not *Z,Z*-isomers. The best matching simulated patterns of *E,Z*-isomers are displayed in Figures 1c,d and 2c,d. Interestingly, nanophase separations between flexible alkyl chains and rigid azobenzenes are suggested for the packing of *E,E*-isomers of both *pAHA* and *oAHA* (Figures 1c and 2c, respectively). The nanophase separation disappears in the self-assembly of the *E,Z*-isomer of *pAHA* (Figure 1d). In the case of *oAHA*, azobenzenes intercalate in a zigzag fashion. Spatial demand of azobenzenes on the surface determines the length *b* of the short lattice axis (Figure 2c): when one of the azobenzenes is switched into the *Z*-form, molecular size is reduced and the packing becomes tighter (Figure 2d). In contrast to *pAHA*, the

**Table 1. Experimental Lattice Constants of *p*AHA and *o*AHA Self-Assembly at the HOPG/TCB Interface**

|  | $a$ (nm) | $b$ (nm) | $\gamma$ (deg) | $\chi^b$ (nm) | $\delta^b$ (deg) | area$^c$ (nm$^2$) | $E_{ads}{}^d$ (kcal/mol) | BE$^e$ (kcal/mol) |
|---|---|---|---|---|---|---|---|---|
| *p*AHA ori | 3.0 ± 0.2 | 2.5 ± 0.1 | 65 ± 5 | - | - | 6.8 ± 0.6 | −210.89$^f$ | −23.35$^f$ |
| *p*AHA irr$^a$ | 4.2 ± 0.1 | 2.52 ± 0.05 | 88 ± 1 | 1.6 ± 0.1 | 11 ± 3 | 5.3 ± 0.2 | −204.57$^g$ | −13.83$^g$ |
| *o*AHA ori | 4.4 ± 0.1 | 2.7 ± 0.1 | 81 ± 3 | 2.0 ± 0.2 | 25 ± 4 | 5.9 ± 0.3 | −211.58$^f$ | −17.27$^f$ |
| *o*AHA irr$^a$ | 5.2 ± 0.2 | 1.77 ± 0.09 | 83 ± 5 | 2.4 ± 0.3 | −4 ± 4 | 4.6 ± 0.3 | −205.72$^g$ | −19.50$^g$ |

$^a$Only formed after irradiation at 366 nm. $^b$Inter-row distance and angle, specified in STM figures. $^c$Area per molecule. $^d$Adsorption energy between molecule and the HOPG surface. Derived from MM/MD simulation. $^e$Intermolecular binding energy. Derived from MM/MD simulation. $^f$Calculated for the *E,E*-form. $^g$Calculated for the *E,Z*-form.

nanophase separation in *o*AHA is retained in the self-assembly of both *E,Z*- and *Z,Z*-isomers (Figure S7). The incremental increase of binding energy with the number of *Z*-units in the *o*AHA molecule indicates that interaction between *Z*-azobenzenes benefits retention of the nanophase separation patterns (Table S2).

It is important to stress that observation of stable self-assemblies of molecules containing *Z*-isomers of azobenzene-based photoswitches at the solid−liquid interface by STM represents a challenging task.[37,40] This is a result of the nonplanarity of the *Z*-isomers and lone-pair electrons of nitrogens interacting with the graphite surfaces, thereby causing molecular desorption. Formation of stable assemblies for different photoactive states without desorption/readsorption of molecules is essential for development of responsive surfaces and devices.[45,49,50] In our case, the packing density increased upon irradiation with UV light, and we did not monitor the presence of regions with fuzzy contrast between domains of different assemblies. It is therefore likely that the physisorbed molecules undergo a process that involves the subsequential desorption, isomerization in solution, and readsorption onto the surface where void space is created by the shrinking of the assemblies. At the same time, some other molecules may undergo isomerization directly on the surface. Moreover, large PAHs such as HBC, namely, NGs, exhibit very high adsorption energy toward HOPG surfaces.[51] In this regard, desorption of molecules from the surface might not occur while molecules may move on the surface during irradiation and rearrange to form the new domains. However, the absence of a monitoring of the switch on the time scale of the event does not allow us to provide a conclusive mechanism for this process. Note also from the MM/MD calculation that absolute values of adsorption energies for the different isomers of *p*AHA and *o*AHA are similar (<9% energy difference from the most to the least stable isomers, see Table S2). Such a scenario is consistent with our observation of self-assembly of the *Z*-azobenzene-containing isomers for both *p*AHA and *o*AHA.

## CONCLUSION

In summary, we have synthesized two model compounds, *p*AHA and *o*AHA, to cast light onto the photoresponsive behavior of large PAHs, as well as NGs, decorated with azobenzenes. UV−vis absorption and $^1$H NMR measurements demonstrated their photoisomerization in solution. STM images and MM/MD simulation of *p*AHA and *o*AHA revealed the photomodulation of self-assembled structures into more compact packings, formed by *Z*-azobenzene-containing isomers at the TCB/HOPG interface. The MM/MD simulation suggests similar nanophase separation between alkyl chains and azobenzenes in all three isomers of *o*AHA while it disappears in the *E,Z*-isomer of *p*AHA. The markedly

different packings of the different isomers of *p*AHA and *o*AHA on the graphite surface provide clear evidence for the potential of using large PAHs, as well as NGs, for the design of new photoresponsive materials that are suitable for the development of switchable surfaces and devices. We are actively working toward gaining a complete understanding on the mechanism of this photomodulated self-assembly and exploring HBC derivatives possessing more azobenzene substituents and higher symmetry.

## ■ EXPERIMENTAL METHODS

**General Details.** All reactions working with air- or moisture-sensitive compounds were carried out under argon atmosphere using standard Schlenk line techniques. Thin layer chromatography (TLC) was performed on silica gel coated aluminum sheets with F254 indicator. Silica gel column chromatography separation was performed with 0.063−0.200 mm particle size. Nuclear magnetic resonance (NMR) spectra were recorded in deuterated solvents using Bruker AVANCE III 500 and Bruker AVANCE III 700 MHz NMR spectrometers. The $^{13}$C NMR spectra were recorded with a spin−echo attached-proton test (APT) sequence with CH, CH$_3$ showing negative signal and C, CH$_2$ showing positive signal. Chemical shifts ($\delta$) were expressed in ppm relative to the residual of solvent (C$_2$D$_2$Cl$_4$ @ 6.00 ppm for $^1$H NMR and 73.78 ppm for $^{13}$C NMR). Coupling constants ($J$) were recorded in Hertz (Hz) with multiplicities explained by the following abbreviations: s = singlet, d = doublet, t = triplet, q = quartet, dd = doublet of doublets, dt = doublet of triplets, m = multiplet, and br = broad. The UV−vis absorption spectra were measured with a PerkinElmer Lambda 900 spectrophotometer in a quartz cuvette (Hellma) with a light path of 1 cm at room temperature. High-resolution mass spectra (HRMS) were recorded by matrix-assisted laser decomposition/ionization (MALDI) using 7,7,8,8-tetracyanoquinodimethane (TCNQ) as matrix with a Bruker Reflex II-TOF spectrometer (MALDI-TOF HRMS).

**Materials.** Unless otherwise noted, all starting materials and reagents were purchased from commercial sources (Alfa Aesar, Sigma-Aldrich, Acros, and TCI) and used without further purification. HBCs **1** and **2** containing two bromo functional groups[43] and the azobenzene boronic ester **3**[44] were synthesized according to the previously published literature procedures.

**Synthesis of *p*AHA.** To a suspension of dibromo-HBC **1** (40 mg, 0.030 mmol), SPhos (4.4 mg, 0.011 mmol), and azobenzene boronic ester **3** (26 mg, 0.084 mmol) in toluene (8 mL) was added a solution of K$_2$CO$_3$ (1.4 g, 10 mmol) in water (1.5 mL) and ethanol (1.5 mL). This mixture was degassed by the freeze−pump−thaw technique (1 cycle). Pd(PPh$_3$)$_4$ (8.0 mg, 0.0069 mmol) was then added to the mixture, which was further degassed by the freeze−pump−thaw technique for another 2 cycles. The mixture was then heated at 40 °C under vigorous stirring for 16 h. After cooling to room temperature, the mixture was poured into methanol. The yellow precipitate was collected by vacuum filtration and washed with methanol and then purified by silica gel column chromatography (two times, eluent: hot toluene) to afford the title compound as a bright yellow solid (32 mg, 69%). $^1$H NMR (500 MHz, C$_2$D$_2$Cl$_4$, 373 K): $\delta$ 8.60−8.40 (br, 4H), 8.35−8.20 (m, 4H), 8.20−8.05 (m, 8H), 8.05−7.95 (m, 8H), 7.75−7.55 (m, 6H), 3.15−2.85 (br, 8H), 2.15−1.90 (br, 8H), 1.85−1.60 (br, 16H), 1.60−1.20 (m, 56H), 1.10−0.85 (br, 12H). $^{13}$C NMR

(126 MHz, C$_2$D$_2$Cl$_4$, 373 K): $\delta$ 153.11, 151.95, 144.02, 139.17, 135.56, 130.54, 129.28, 128.86, 128.59, 127.72, 123.47, 122.90, 122.08, 121.99, 120.70, 120.66, 120.39, 118.67, 118.50, 118.42, 36.83, 31.70, 31.58, 29.99, 29.78, 29.71, 29.67, 29.62, 29.49, 29.12, 22.39, 13.74. HRMS (MALDI-TOF) Mass. Calcd. for C$_{114}$H$_{130}$N$_4$ [M]$^+$ 1555.0296. Found [M]$^+$ 1555.0505.

**Synthesis of *o*AHA.** To a suspension of dibromo-HBC **2** (45 mg, 0.034 mmol), SPhos (5.4 mg, 0.014 mmol), and azobenzene boronic ester **3** (41 mg, 0.13 mmol) in toluene (6 mL) was added a solution of K$_2$CO$_3$ (0.7 g, 5 mmol) in water (1 mL) and ethanol (1 mL). This mixture was degassed by the freeze−pump−thaw technique (1 cycle). Pd(PPh$_3$)$_4$ (7.6 mg, 0.0066 mmol) was then added to the mixture, which was further degassed by the freeze−pump−thaw technique for another 2 cycles. The mixture was then heated at 40 °C under vigorous stirring for 16 h. After cooling to a room temperature, the mixture was poured into methanol. The yellow precipitates were collected by vacuum filtration and washed with methanol and then purified by silica gel column chromatography (two times, eluent: hot toluene) to afford the title compound as a brownish solid (38 mg, 73%). $^1$H NMR (500 MHz, C$_2$D$_2$Cl$_4$, 373 K): $\delta$ 8.20−8.05 (m, 8H), 8.00−7.87 (br, 2H), 7.85−7.80 (br, 2H), 7.80−7.76 (br, 2H), 7.76−7.71 (br, 2H), 7.71−7.60 (m, 12H), 7.58−7.50 (br, 2H), 3.00−2.80 (br, 4H), 2.80−2.65 (br, 4H), 2.05−1.93 (br, 4H), 1.93−1.78 (br, 4H), 1.78−1.20 (m, 72H), 1.10−0.90 (m, 12H). $^{13}$C NMR (126 MHz, C$_2$D$_2$Cl$_4$, 373 K): $\delta$ 153.15, 151.72, 143.32, 138.73, 138.51, 134.22, 130.48, 128.85, 128.61, 128.55, 128.27, 128.20, 128.01, 127.91, 127.19, 123.24, 122.90, 122.65, 121.68, 121.48, 120.27, 120.20, 119.85, 118.09, 118.00, 117.80, 117.62, 117.10, 36.89, 36.66, 31.74, 31.63, 31.35, 30.11, 30.09, 29.84, 29.74, 29.70, 29.68, 29.61, 29.54, 29.42, 29.17, 22.43, 13.78. HRMS (MALDI-TOF) Mass. Calcd. for C$_{114}$H$_{130}$N$_4$ [M]$^+$ 1555.0296. Found [M]$^+$ 1555.0420.

**Photoswitching in Solution.** The photoswitching in solution was conducted by direct irradiation of a THF solution of *p*AHA or *o*AHA in a quartz cuvette used for UV−vis absorption spectral measurement. The absorption spectra were directly recorded using a UV−vis spectrophotometer after irradiation. The light source used for switching was a Mercury arc lamp (HBO 200W/2, OSRAM). The irradiation wavelength was controlled by using optical filters (Schott Glaswerke). More details of experimets can be found in the Supporting Information.

**STM Investigation.** The STM imaging was conducted at ambient pressure and room temperature at constant current mode with a Veeco Multimode III (Bruker) connected with a STM head (tip: mechanically cut Pt/Ir wire, 4:1, $\theta = 0.25$ mm, Goodfellow) and a 1 $\mu$m piezoelectric scanner (A-Piezo, Veeco). The substrates (HOPG, Momentive Performance) were glued on (silver conductive paint, Aldrich) a metal disk (Ted Pella) that magnetically attached to the STM base. In our instrumental configuration, the sample is grounded. The experiments were performed at the solid/liquid interface between the HOPG and a drop (4 $\mu$L) of TCB solution of the molecule under investigation. The photocontrolled assembly was achieved by in situ irradiation of the solution on the HOPG substrate with optical fiber-coupled LED light source (ThorLabs, 365 nm, $P_\text{d} = 2$ mW cm$^{-2}$) by placing the collimator lens at a distance of 5 cm for 3 min. The raw STM data were processed by SPIP (Image Metrology). Drift of every image was calibrated by the images of the HOPG crystal lattice in situ ($V_\text{T} = 60$ mV, $I_\text{T} = 20$ pA). The unit cell constants were estimated from the average of multiple images (*p*AHA *ori*: 75, *p*AHA *irr*: 18, *p*AHA *irr2*: 6, *o*AHA *ori*: 13, *o*AHA *ori2*: 20, *o*AHA *irr*: 26).

**MM/MD Simulations.** The methodology employed in the MM/MD simulation is the same as the one used in our previous work for multiazobenzene compounds.[37] The details about the description of the modifed Dreiding force field[52] used to reproduce the geometries of the multiazobenzene groups adsorbed on graphite are given in the previously mentioned work. All the MM/MD simulations were performed using Materials Studio 7.0 package.[53] Details of the simulation methods and description can be found in the Supporting Information.

## ASSOCIATED CONTENT

**Ⓢ Supporting Information**

The Supporting Information is available free of charge on the ACS Publications website at DOI: 10.1021/acs.chemmater.9b01535.

> $^1$H NMR and $^{13}$C NMR characterization of the materials, UV−vis absorption spectra, additional STM images and lattice constants, and summary of MM/MD figures and lattice constants (PDF)

## AUTHOR INFORMATION

**Corresponding Authors**
*(A.N.) E-mail: narita@mpip-mainz.mpg.de.
*(P.S.) E-mail: samori@unistra.fr.
*(K.M.) E-mail: muellen@mpip-mainz.mpg.de.
**ORCID** Ⓘ
Michal Valášek: 0000-0001-9382-6327
Marcel Mayor: 0000-0002-8094-7813
Jérôme Cornil: 0000-0002-5479-4227
Akimitsu Narita: 0000-0002-3625-522X
Paolo Samorì: 0000-0001-6256-8281
Klaus Müllen: 0000-0001-6630-8786
**Notes**
The authors declare no competing financial interest.

## REFERENCES

(1) Narita, A.; Wang, X. Y.; Feng, X.; Müllen, K. New Advances in Nanographene Chemistry. *Chem. Soc. Rev.* **2015**, 44 (18), 6616−6643.

(2) Wang, X.-Y.; Narita, A.; Müllen, K. Precision Synthesis versus Bulk-Scale Fabrication of Graphenes. *Nat. Rev. Chem.* **2018**, 2 (1), 0100.

(3) Narita, A.; Chen, Z.; Chen, Q.; Müllen, K. Solution and On-Surface Synthesis of Structurally Defined Graphene Nanoribbons as a New Family of Semiconductors. *Chem. Sci.* **2019**, 10 (4), 964−975.

(4) Chen, Q.; Brambilla, L.; Daukiya, L.; Mali, K. S.; De Feyter, S.; Tommasini, M.; Müllen, K.; Narita, A. Synthesis of Triply Fused Porphyrin-Nanographene Conjugates. *Angew. Chem., Int. Ed.* **2018**, 57 (35), 11233−11237.

(5) Yen, H. J.; Tsai, H.; Zhou, M.; Holby, E. F.; Choudhury, S.; Chen, A.; Adamska, L.; Tretiak, S.; Sanchez, T.; Iyer, S.; et al. Structurally Defined 3D Nanographene Assemblies via Bottom-Up Chemical Synthesis for Highly Efficient Lithium Storage. *Adv. Mater.* **2016**, 28 (46), 10250−10256.

(6) Wu, J.; Pisula, W.; Müllen, K. Graphenes as Potential Material for Electronics. *Chem. Rev.* **2007**, 107 (3), 718−747.

(7) Wang, Y.; Yin, Z.; Zhu, Y.; Gu, J.; Li, Y.; Wang, J. Hexapole [9]Helicene. *Angew. Chem., Int. Ed.* **2019**, 58 (2), 587−591.

(8) Evans, P. J.; Ouyang, J.; Favereau, L.; Crassous, J.; Fernández, I.; Perles, J.; Martín, N. Synthesis of a Helical Bilayer Nanographene. *Angew. Chem., Int. Ed.* **2018**, 57 (23), 6774−6779.

(9) Ziogos, O. G.; Konstantinopoulos, S.; Tsetseris, L.; Theodorou, D. N. Computational Studies of Nanographene Systems: Extended

Discotics, Covalently Linked "Supermolecules," and Functionalized Supramolecular Assemblies. *J. Phys. Chem. C* **2018**, *122* (32), 18715−18731.

(10) Feng, X.; Pisula, W.; Kudernac, T.; Wu, D.; Zhi, L.; De Feyter, S.; Müllen, K. Controlled Self-Assembly of C3-Symmetric Hexa-Peri-Hexabenzocoronenes with Alternating Hydrophilic and Hydrophobic Substituents in Solution, in the Bulk, and on a Surface. *J. Am. Chem. Soc.* **2009**, *131* (12), 4439−4448.

(11) Zhou, Y.; Zhang, M. Y.; Gu, K. H.; Zhu, Y. F.; Fan, X. H.; Shen, Z. Facile Synthesis and Phase Behaviors of Monofunctionalized Hexa-Peri-Hexabenzocoronenes. *Asian J. Org. Chem.* **2015**, *4* (8), 746−755.

(12) Wong, W. W. H.; Singh, T. B.; Vak, D.; Pisula, W.; Yan, C.; Feng, X.; Williams, E. L.; Chan, K. L.; Mao, Q.; Jones, D. J.; et al. Solution Processable Fluorenyl Hexa-Peri-Hexabenzocoronenes in Organic Field-Effect Transistors and Solar Cells. *Adv. Funct. Mater.* **2010**, *20* (6), 927−928.

(13) Gu, K.; Zhang, M.; Zhou, Y.; Han, M.; Zhang, W.; Shen, Z.; Fan, X. Hierarchical Self-Assembly of Disc-Rod Shape Amphiphiles Having Hexa-Peri-Hexabenzocoronene and a Relatively Long Rod. *Langmuir* **2017**, *33* (13), 3311−3316.

(14) Hu, Y.; Dössel, L. F.; Wang, X.-Y.; Mahesh, S.; Pisula, W.; De Feyter, S.; Feng, X.; Müllen, K.; Narita, A. Synthesis, Photophysical Characterization, and Self-Assembly of Hexa- Peri -Hexabenzocoronene/Benzothiadiazole Donor-Acceptor Structure. *ChemPlusChem* **2017**, *82* (7), 1030−1033.

(15) Keerthi, A.; Hou, I. C. Y.; Marszalek, T.; Pisula, W.; Baumgarten, M.; Narita, A. Hexa-Peri-Hexabenzocoronene with Different Acceptor Units for Tuning Optoelectronic Properties. *Chem. - Asian J.* **2016**, *11* (19), 2710−2714.

(16) Hinkel, F.; Cho, D.; Pisula, W.; Baumgarten, M.; Müllen, K. Alternating Donor-Acceptor Arrays from Hexa-Perihexabenzocoronene and Benzothiadiazole: Synthesis, Optical Properties, and Self-Assembly. *Chem. - Eur. J.* **2015**, *21* (1), 86−90.

(17) Wu, S. H.; Chen, H. H. Self-Assembling Behavior of Binary Mixture of Hexa-Peri-Hexabenzocoronene Derivatives with Different Molecular Symmetry. *Tetrahedron* **2019**, *75* (2), 220−229.

(18) Dumslaff, T.; Yang, B.; Maghsoumi, A.; Velpula, G.; Mali, K. S.; Castiglioni, C.; De Feyter, S.; Tommasini, M.; Narita, A.; Feng, X.; et al. Adding Four Extra K-Regions to Hexa-Peri-Hexabenzocoronene. *J. Am. Chem. Soc.* **2016**, *138* (14), 4726−4729.

(19) Ai, M.; Groeper, S.; Zhuang, W.; Dou, X.; Feng, X.; Müllen, K.; Rabe, J. P. Optical Switching Studies of an Azobenzene Rigidly Linked to a Hexa-Peri-Hexabenzocoronene Derivative in Solution and at a Solid-Liquid Interface. *Appl. Phys. A: Mater. Sci. Process.* **2008**, *93* (2), 277−283.

(20) Pisula, W.; Zorn, M.; Chang, J. Y.; Müllen, K.; Zentel, R. Liquid Crystalline Ordering and Charge Transport In Semiconducting Materials. *Macromol. Rapid Commun.* **2009**, *30* (14), 1179−1202.

(21) Fleischmann, E. K.; Zentel, R. Liquid-Crystalline Ordering as a Concept in Materials Science: From Semiconductors to Stimuli-Responsive Devices. *Angew. Chem., Int. Ed.* **2013**, *52* (34), 8810−8827.

(22) Oda, K.; Hiroto, S.; Shinokubo, H. NIR Mechanochromic Behaviours of a Tetracyanoethylene-Bridged Hexa-: Peri-Hexabenzocoronene Dimer and Trimer through Dissociation of C-C Bonds. *J. Mater. Chem. C* **2017**, *5* (22), 5310−5315.

(23) Feringa, B. L.; Browne, W. R. *Molecular Switches*, 2nd.; Feringa, B. L., Browne, W. R., Eds.; Wiley-VCH Verlag GmbH & Co. KGaA: Weinheim, Germany, 2011; Vol. 1.

(24) Lubbe, A. S.; Szymanski, W.; Feringa, B. L. Recent Developments in Reversible Photoregulation of Oligonucleotide Structure and Function. *Chem. Soc. Rev.* **2017**, *46* (4), 1052−1079.

(25) Balzani, V.; Credi, A.; Venturi, M. *Molecular Devices and Machines: Concepts and Perspectives for the Nanoworld*; 2nd ed.; Wiley-VCH Verlag GmbH & Co. KGaA: Weinheim, Germany, 2008; Vol. 2.

(26) Zhang, X.; Hou, L.; Samorì, P. Coupling Carbon Nanomaterials with Photochromic Molecules for the Generation of Optically Responsive Materials. *Nat. Commun.* **2016**, *7*, 11118.

(27) Barrett, C. J.; Mamiya, J. I.; Yager, K. G.; Ikeda, T. Photo-Mechanical Effects in Azobenzene-Containing Soft Materials. *Soft Matter* **2007**, *3* (10), 1249−1261.

(28) Naumov, P.; Chizhik, S.; Panda, M. K.; Nath, N. K.; Boldyreva, E. Mechanically Responsive Molecular Crystals. *Chem. Rev.* **2015**, *115* (22), 12440−12490.

(29) Bisoyi, H. K.; Li, Q. Light-Driven Liquid Crystalline Materials: From Photo-Induced Phase Transitions and Property Modulations to Applications. *Chem. Rev.* **2016**, *116* (24), 15089−15166.

(30) Yagai, S.; Kitamura, A. Recent Advances in Photoresponsive Supramolecular Self-Assemblies. *Chem. Soc. Rev.* **2008**, *37* (8), 1520−1529.

(31) Orgiu, E.; Samorì, P. 25th Anniversary Article: Organic Electronics Marries Photochromism: Generation of Multifunctional Interfaces, Materials, and Devices. *Adv. Mater.* **2014**, *26* (12), 1827−1844.

(32) Scheil, K.; Gopakumar, T. G.; Bahrenburg, J.; Temps, F.; Maurer, R. J.; Reuter, K.; Berndt, R. Switching of an Azobenzene-Tripod Molecule on Ag(111). *J. Phys. Chem. Lett.* **2016**, *7* (11), 2080−2084.

(33) Jaekel, S.; Richter, A.; Lindner, R.; Bechstein, R.; Nacci, C.; Hecht, S.; Kühnle, A.; Grill, L. Reversible and Efficient Light-Induced Molecular Switching on an Insulator Surface. *ACS Nano* **2018**, *12* (2), 1821−1828.

(34) Mielke, J.; Selvanathan, S.; Peters, M.; Schwarz, J.; Hecht, S.; Grill, L. Molecules with Multiple Switching Units on a Au(111) Surface: Self-Organization and Single-Molecule Manipulation. *J. Phys.: Condens. Matter* **2012**, *24* (39), 394013.

(35) Tegeder, P. Optically and Thermally Induced Molecular Switching Processes at Metal Surfaces. *J. Phys.: Condens. Matter* **2012**, *24* (39), 394001.

(36) Nacci, C.; Baroncini, M.; Credi, A.; Grill, L. Reversible Photoswitching and Isomer-Dependent Diffusion of Single Azobenzene Tetramers on a Metal Surface. *Angew. Chem., Int. Ed.* **2018**, *57* (46), 15034−15039.

(37) Galanti, A.; Diez-Cabanes, V.; Santoro, J.; Valášek, M.; Minoia, A.; Mayor, M.; Cornil, J.; Samorì, P. Electronic Decoupling in C3-Symmetrical Light-Responsive Tris(Azobenzene) Scaffolds: Self-Assembly and Multiphotochromism. *J. Am. Chem. Soc.* **2018**, *140* (47), 16062−16070.

(38) Frath, D.; Yokoyama, S.; Hirose, T.; Matsuda, K. Photoresponsive Supramolecular Self-Assemblies at the Liquid/Solid Interface. *J. Photochem. Photobiol., C* **2018**, *34*, 29−40.

(39) Garah, M. El; Borré, E.; Ciesielski, A.; Dianat, A.; Gutierrez, R.; Cuniberti, G.; Bellemin-Laponnaz, S.; Mauro, M.; Samorì, P. Light-Induced Contraction/Expansion of 1D Photoswitchable Metallopolymer Monitored at the Solid−Liquid Interface. *Small* **2017**, *13* (40), 1701790.

(40) Zeitouny, J.; Aurisicchio, C.; Bonifazi, D.; De Zorzi, R.; Geremia, S.; Bonini, M.; Palma, C. A.; Samorì, P.; Listorti, A.; Belbakra, A.; et al. Photoinduced Structural Modifications in Multicomponent Architectures Containing Azobenzene Moieties as Photoswitchable Core. *J. Mater. Chem.* **2009**, *19* (27), 4715−4724.

(41) Liu, Y.; Mu, L.; Liu, B.; Kong, J. Controlled Switchable Surface. *Chem. - Eur. J.* **2005**, *11* (9), 2622−2631.

(42) Tahara, K.; Inukai, K.; Adisoejoso, J.; Yamaga, H.; Balandina, T.; Blunt, M. O.; De Feyter, S.; Tobe, Y. Tailoring Surface-Confined Nanopores with Photoresponsive Groups. *Angew. Chem., Int. Ed.* **2013**, *52* (32), 8373−8376.

(43) Ito, S.; Wehmeier, M.; Brand, J. D.; Kübel, C.; Epsch, R.; Rabe, J. P.; Müllen, K. Synthesis and Self-Assembly of Functionalized Hexa-Peri-Hexabenzocoronenes. *Chem. - Eur. J.* **2000**, *6* (23), 4327−4342.

(44) Harvey, J. H.; Butler, B. K.; Trauner, D. Functionalized Azobenzenes through Cross-Coupling with Organotrifluoroborates. *Tetrahedron Lett.* **2007**, *48* (9), 1661−1664.

(45) Bléger, D.; Ciesielski, A.; Samorì, P.; Hecht, S. Photoswitching Vertically Oriented Azobenzene Self-Assembled Monolayers at the Solid-Liquid Interface. *Chem. - Eur. J.* **2010**, *16* (48), 14256−14260.

(46) Samorí, P.; Fechtenkötter, A.; Jäckel, F.; Böhme, T.; Müllen, K.; Rabe, J. P. Supramolecular Staircase via Self-Assembly of Disklike Molecules at the Solid-Liquid Interface. *J. Am. Chem. Soc.* **2001**, *123* (46), 11462−11467.

(47) Piot, L.; Marchenko, A.; Wu, J.; Müllen, K.; Fichou, D. Structural Evolution of Hexa-Peri-Hexabenzocoronene Adlayers in Heteroepitaxy on n-Pentacontane Template Monolayers. *J. Am. Chem. Soc.* **2005**, *127* (46), 16245−16250.

(48) Müllen, K.; Fichou, D.; Silly, F.; Marie, C.; Tortech, L. Tuning the Packing Density of 2D Supramolecular Self-Assemblies at the Solid-Liquid Interface Using Variable Temperature. *ACS Nano* **2010**, *4* (3), 1288−1292.

(49) Cojal González, J. D.; Iyoda, M.; Rabe, J. P. Reversible Photoisomerization of Monolayers of $\pi$-Expanded Oligothiophene Macrocycles at Solid-Liquid Interfaces. *Angew. Chem., Int. Ed.* **2018**, *57* (52), 17038−17042.

(50) Tahara, K.; Inukai, K.; Adisoejoso, J.; Yamaga, H.; Balandina, T.; Blunt, M. O.; De Feyter, S.; Tobe, Y. Tailoring Surface-Confined Nanopores with Photoresponsive Groups. *Angew. Chem., Int. Ed.* **2013**, *52* (32), 8373−8376.

(51) Weippert, J.; Hauns, J.; Bachmann, J.; Böttcher, A.; Yao, X.; Yang, B.; Narita, A.; Müllen, K.; Kappes, M. M. A TPD-Based Determination of the Graphite Interlayer Cohesion Energy. *J. Chem. Phys.* **2018**, *149* (19), 194701.

(52) Mayo, S. L.; Olafson, B. D.; Goddard, W. A. DREIDING: A Generic Force Field for Molecular Simulations. *J. Phys. Chem.* **1990**, *94* (26), 8897−8909.

(53) *MS Modeling*, V7; Accelrys Software Inc.: San Diego, CA, 2015.